JOURNAL OF APPLIED ELECTROCHEMISTRY **27** (1997) 568–572

Electrochemical investigation of the Ni–Cu–Mo electrodeposition system

E. BELTOWSKA-LEHMAN

Institute of Metallurgy and Materials Science, Polish Academy of Sciences, ul. Reymonta 25, 30-059 Krakow, Poland

E. CHASSAING

Centre d'Etudes de Chimie Métallurgique, CNRS, 94407 Vitry-sur-Seine Cedex, France

Received 12 June 1995; revised 9 December 1996

The kinetics of Ni–Cu–Mo alloy deposition has been investigated by means of steady-state polarization measurements. Strong interactions between the three discharging metals occur: nickel induces molybdenum deposition but its discharge is markedly inhibited by molybdenum. Copper deposition has a depolarizing effect on Ni–Mo discharge. Hydrogen evolution is associated with molybdenum deposition. The electrocrystallization process is dominated by the Ni–Mo codischarge kinetics.

1. Introduction

Alloys containing molybdenum are characterized by a high hardness and high wear and corrosion resistance [1]. Ni–Cu alloys containing about 30 wt % Cu, such as Monel 400 and Ni–Mo alloys with 26 wt % Mo, such as Hastelloy B are known to be highly corrosion resistant in many aggressive environments [1]. Ternary nickel-based alloys containing copper and molybdenum would have high corrosion resistance. However, these alloys are difficult to prepare by conventional metallothermic methods because of the lack of solubility of molybdenum and copper and of the large differences in their melting points. Electrodeposition is an alternative method for the preparation of such alloys.

In a previous work we have developed conditions to electrodeposit Ni–Cu–Mo alloys [2]. The effect of electrolyte composition (pH, metallic species and complexing agent concentrations) has been investigated on the alloy composition, the current efficiency and deposit quality [2]. To improve the layer quality, pulse plating was studied and pulse parameters have been determined which allow preparation of good quality layers [3].

The electrocrystallization process of these ternary alloys is interesting from a theoretical point of view. Indeed, it combines two different codeposition systems:

(i) The Ni–Cu system is considered to be of the 'normal' codeposition type according to Brenner's classification [4]. However the more recent classification as charge-coupled codeposition system would be more appropriate, since interactions between the discharging metals may occur during the deposition [5].

(ii) The Ni–Mo system is called an induced system because molybdenum cannot be separately deposited but its discharge can be induced only by iron-group metals [4, 5]. In spite of many attempts to understand the electrocrystallization mechanism of induced codeposition systems, no unique theory accounts for all the characteristics of the process [4–14]. The present work is aimed at a better understanding of the kinetics of Ni–Cu–Mo alloy deposition. The ternary alloy discharge is compared to separate nickel, copper deposition and to binary Ni–Cu and Ni–Mo codeposition systems. As is well known, Cu and Mo cannot readily codeposit [4], hence we did not investigate this system.

2. Experimental procedure

Complex ammonia–citrate electrolytes were used to bring the deposition potentials of the metals closer. The solutions contained nickel and copper sulfate, sodium molybdate and sodium citrate. The pH was adjusted to 7 by addition of ammonia. Separate Ni, Cu and binary Ni–Cu, Ni–Mo systems were also investigated. The electrolyte compositions are given in Table 1. The electrolysis was carried out in a 750 ml cell at 25 °C.

A low carbon–steel disc (0.028 dm^2) rotating up to 86 rad s^{-1}, was used. It was chemically polished prior to each experiment. A platinum sheet was used as anode. The potentials were measured with respect to a saturated calomel electrode (SCE) via a Luggin capillary located 1 mm from the disc. Chemical analysis of the deposits was carried out by atomic absorption spectroscopy.

The global and partial polarization curves were determined from coulometric measurements and from the deposit composition. The maximum relative error on the partial currents was about 7%. The electrochemical impedance was measured in the range 60 kHz to 5 mHz at various polarizations.

0021-891X © 1997 Chapman & Hall

Table 1. Electrolyte compositions (mol dm^{-3})

Electrolyte	*System*	*$NiSO_4$*	*$CuSO_4$*	*Na_2MoO_4*	*$Na_3C_6H_5O_7$*
1	Ni	0.75			0.45
2	Cu		0.06		0.45
3	Ni–Cu	0.75	0.06		0.45
4	Ni–Mo	0.75		0.02	0.45
5	Ni–Cu–Mo	0.75	0.06	0.02	0.45

3. Results

3.1. *Steady-state polarization curves at set rotation speeds*

The global and partial polarization curves were investigated for various electrode rotation speeds. These curves were compared to the polarization curves obtained for the separate discharge of nickel, copper and the binary Ni–Cu and Ni–Mo systems. Figure 1 shows an example of the polarization curves of the ternary alloy discharge recorded at 34 rad s^{-1}. At low polarization, that is, −0.8 to −1 V vs SCE, copper discharge (curve (b)) and hydrogen evolution (curve (e)) are the main reactions ($i_H = i_{Cu} =$ 0.6 A dm^{-2}, at $E = -1.0$ V), the Ni and Mo partial currents (curves (c) and (d)) are very low ($i_{Ni} \approx i_{Mo} \approx$ 0.06 A dm^{-2} at $E = -1.0$ V). In the range −1.0 to −1.4 V hydrogen evolution (curve (e)) is the major reaction. With increasing polarization the partial current for hydrogen evolution rapidly decreases and both Ni and Mo partial currents increase, as already observed for the binary Ni–Mo system [9]. At still more negative potentials nickel discharge becomes the predominant reaction (curve (c)).

Figure 2 shows nickel partial polarization curves during its separate discharge (curve (a)), its codeposition with copper (curve (b)), with molybdenum (curve (c)), and with copper and nickel (ternary alloy system) (curve (d)). The codischarge of copper (curve (b)) slightly increases the polarization of nickel discharge (curve (a)). The codeposition of molybdenum drastically inhibits the nickel discharge, the polarization curve is shifted to much more negative potentials (curve (c)), whereas the addition of copper has a depolarizing effect (curve (d)).

The hydrogen partial current is rather low for the separate discharge (Fig. 3, curve (a)) and the binary Ni–Cu system (curve (b)). The codischarge of molybdenum considerably increases the hydrogen evolution (curve (c) for Ni–Mo and curve (d) for Ni–Cu–Mo). The polarization curve of hydrogen exhibits a maximum, as already observed in the electrocrystallization of Ni–Mo alloys [9]. The presence of copper strongly decreases hydrogen evolution and shifts the maximum to less negative values.

3.2. *Effect of electrode rotation speed on polarization curves*

The effect of the electrode rotation speed on the global polarization curve is not pronounced except at large polarization ($E < -1.5$ V vs SCE). For copper deposition, a mixed activation–diffusion control is observed at low polarization. A diffusion-controlled discharge is obtained at potentials more negative than −1.5 V vs SCE where a linear dependence of the partial current as a function of the square root of the electrode rotation speed is observed. The apparent diffusion coefficient in the ternary alloy system is 10^{-6} cm^2 s^{-1}: that is, of the same order of magnitude as in the binary Ni–Cu system [16]. It is much lower than in the copper sulfate/citrate solutions [17] and in the pure copper sulfate electrolytes [18]. This is

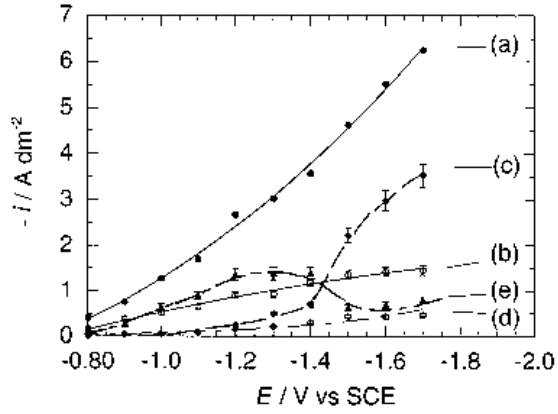

Fig. 1. Steady-state polarization curves recorded at 34 rad s^{-1} for the ternary Ni–Cu–Mo deposition (electrolyte 5). Key: (a) global polarization curve; (b) partial polarization curve for copper discharge; (c) partial polarization curve for nickel discharge; (d) partial polarization curve for molybdenum discharge; and (e) partial polarization curve for hydrogen discharge.

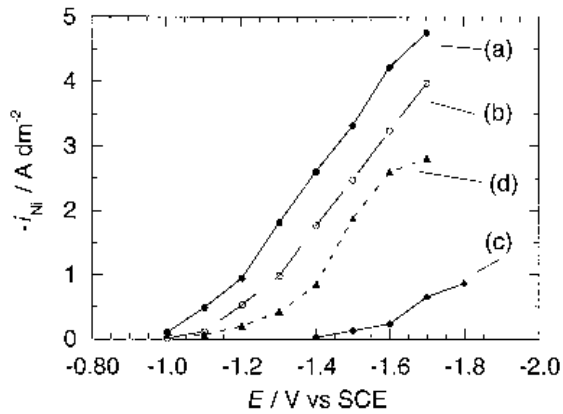

Fig. 2. Partial polarization curves for nickel discharge recorded at 68 rad s^{-1}. Key: (a) separate nickel discharge (electrolyte 1); (b) discharge in the presence of copper (electrolyte 3); (c) discharge in the presence of molybdenum (electrolyte 4); and (d) discharge in the presence of copper and molybdenum (electrolyte 5).

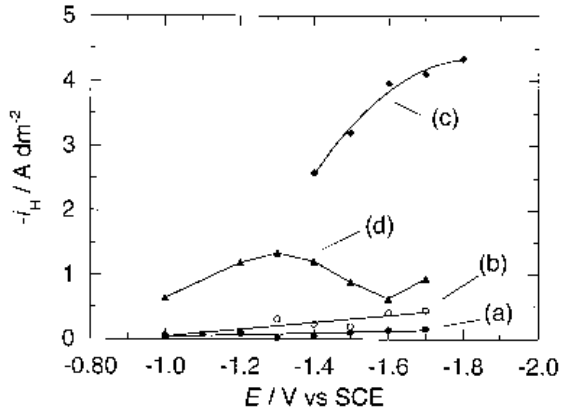

Fig. 3. Partial polarization curves for hydrogen evolution recorded at 68 rad s^{-1}. Key: (a) separate nickel discharge (electrolyte 1); (b) discharge in Ni–Cu system (electrolyte 3); (c) discharge in Ni–Mo system (electrolyte 4); and (d) discharge in Ni–Cu–Mo (electrolyte 5).

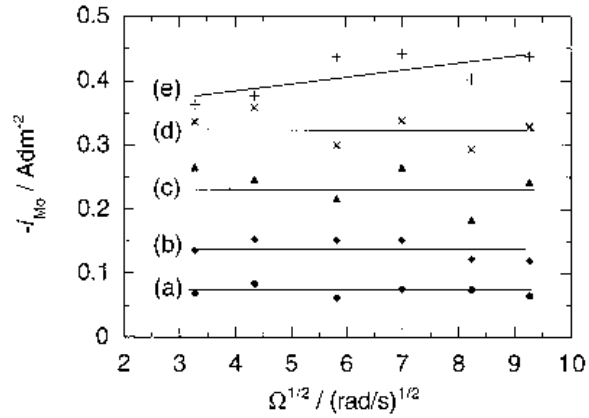

Fig. 5. Effect of electrode rotation speed on the partial polarization curve for molybdenum discharge in ternary system (electrolyte 5). *E*: (a) −1.0, (b) −1.2, (c) −1.3, (d) −1.4 and (e) −1.5 V vs SCE.

probably related to the presence of complexed copper species, particularly of heteronuclear citrate of Ni(II) and Cu(II) such as $[Cu,Ni(C_6H_4O_7)_2]^{4-}$ [15, 19].

Figure 4 shows that the electrode rotation speed has no influence on the separate nickel discharge (curve (a)) nor on its codischarge with copper (curve (b)), as already observed [10]. By contrast, during codeposition with molybdenum (curve (c)) and, to a lesser extent, in the ternary alloy deposition (curve (d)), the partial nickel current decreases as the rotation is increased. A comparison with Fig. 2 clearly shows that the codischarge of molybdenum inhibits nickel discharge and that the blocking species is mass transported towards the electrode.

The partial molybdenum current density does not depend on the rotation speed in the ternary Ni–Cu–Mo system, as shown in Fig. 5, except at high overpotentials where molybdenum discharge becomes diffusion controlled (for $E < -1.5$ V vs SCE, curve (e)).

The partial current density for hydrogen discharge does not depend on rotation speed during separate Ni deposition and in the binary Ni–Cu system. By contrast, hydrogen evolution markedly increases with rotation in the binary Ni–Mo system. In the ternary Ni–Cu–Mo system (Fig. 6), as already mentioned, the polarization curve exhibits a maximum. The maximum is slightly shifted to more negative potentials when the rotation speed is increased. At potentials more negative than the maximum, the current increases with rotation speed (Fig. 6).

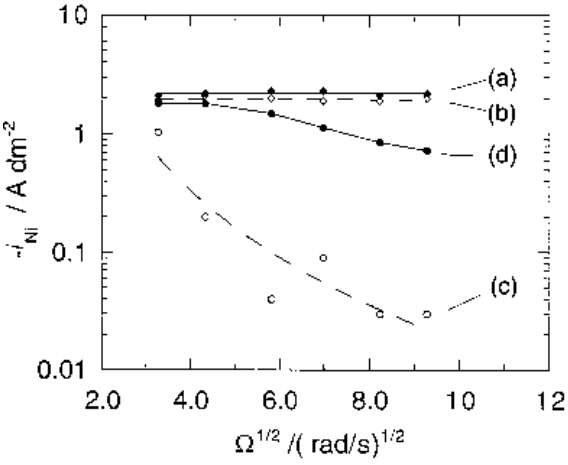

Fig. 4. Effect of electrode rotation speed on the partial polarization curve for nickel discharge at $E = -1.4$ V vs SCE. Key: (a) separate nickel discharge (electrolyte 1); (b) discharge in Ni–Cu system (electrolyte 3); (c) discharge in Ni–Mo system (electrolyte 4); and (d) discharge in Ni–Cu–Mo (electrolyte 5).

3.3. *Electrochemical impedance*

The electrochemical impedance was measured for various electrode rotation speeds along the polarization curve. The impedance plots exhibit a large capacitive loop with an inflection in the high frequency domain (Fig. 7). The capacitance calculated from the frequency at the apex of the capacitive loop lies around 30 mF cm^{-2}, i.e. much larger than the value for the double layer capacitance. This large value, and the high frequency inflection, is indicative of the fact that the charge transfer occurs through a porous layer [20]. This layer may be an oxide or a hydroxide layer resulting from a local pH increase. A similar behaviour has been observed during Ni–Mo electrocrystallization and attributed to the formation of a

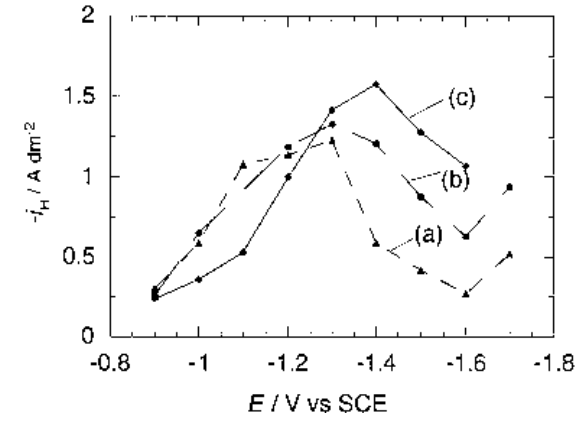

Fig. 6. Effect of electrode rotation speed on the partial polarization curve for hydrogen evolution.: (a) 19; (b) 68 and (c) 87 rad s^{-1}.

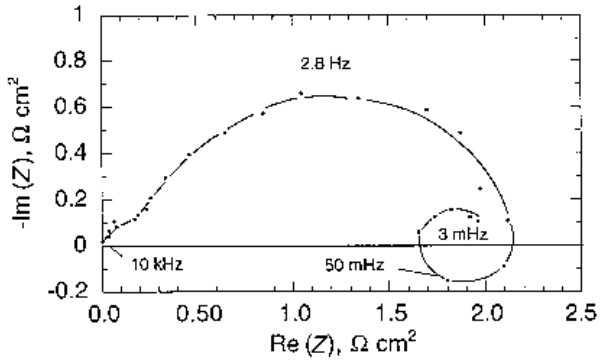

Fig. 7. Impedance diagram recorded in electrolyte 5 at a current density of 4 A dm^{-2}, for an electrode rotation speed of 105 rad s^{-1}.

molybdenum oxide [9]. A small inductive feature is observed whose characteristic frequency lies around 10 mHz. No marked effect of the electrode rotation speed on the impedance is observed.

3.4. *Composition of Ni–Cu–Mo layers and faradaic efficiency*

The composition of the alloys results from the polarization behaviour (Fig. 8). When the potential is shifted towards more negative values, the copper content rapidly decreases, whereas the nickel content increases. The molybdenum content shows a slight maximum at intermediate polarization; it is much lower than in the case of binary Ni–Mo deposition. Except at low overpotentials the current efficiency for Ni–Cu–Mo discharge shows the same tendency as the nickel content in the deposit. It is lower than for Ni–Cu system but much higher than for Ni–Mo.

4. Discussion

The present investigation shows that during ternary Ni–Cu–Mo discharge strong interactions between the three depositing metals and with hydrogenated species occur. The discharge process is dominated by the Ni–Mo codeposition kinetics.

Four polarization ranges can be distinguished:

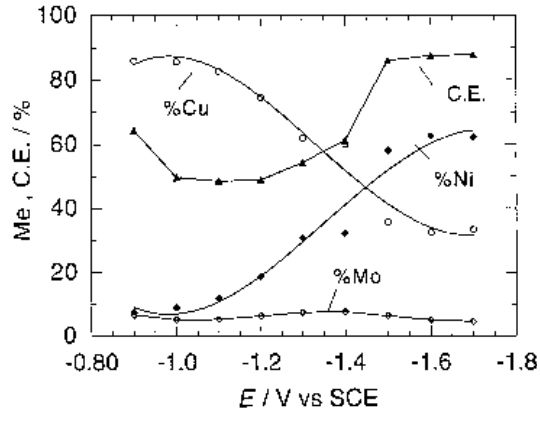

Fig. 8. Metal content and current efficiency as function of deposition potential in electrolyte 5. Rotation speed 34 rad s^{-1}.

(i) At low overpotentials (–0.8 to –1.0 V vs SCE) copper discharge is the main reaction (deposits with up to 86 wt % Cu).
(ii) In the range –1.0 to –1.4 V vs SCE, hydrogen evolution is important. It is likely that the co-discharge of molybdenum proceeds in the ternary alloy system as in binary Ni–Mo [9]: evolution of hydrogen from the citrate complexes and formation of molybdenum oxides, which blocks the electrode area. If hydrogen evolution was the result of water decomposition without any interaction with the discharging metals, the hydrogen partial polarization curve would be a continuously increasing curve with potential, showing a quasi-Tafel behaviour. The presence of a maximum shows that interactions occur between hydrogen species and surface compounds.
(iii) With increasing polarization the presence of the Ni^{2+} species would induce the formation of a mixed Ni–Mo oxide and allow the reduction of the molybdate species.
(iv) At still more negative potentials the crystallization process becomes controlled by diffusion of both molybdenum and copper species.

The NiCuMo electrodeposition system combines two different electrocrystallization mechanisms according to Brenner's classification:

(i) the Ni–Cu system is considered normal [4]. Copper and nickel can be separately deposited, their codeposition is achieved due to complexing agents such as citrate and ammonia. It has been shown that interaction occurs between the two discharging metals, hence the classification in 'charge transfer-coupled system' is more appropriate [5]. A reaction model has been developed based on polarization and electrochemical impedance investigations, which considered the two-step discharge of nickel and copper species occurring in parallel at the electrode.
(ii) the Ni–Mo system is known as an induced codeposition system since molybdenum, which cannot separately discharge in aqueous solution, can codeposit with an iron-group metal such as nickel. Several investigations have been carried out to try to understand the Ni–Mo induced codeposition [6, 7, 10–14]. Chassaing *et al.* considered the multistep reduction of the molybdic species. Because of the presence of Ni^{2+} ions a mixed Ni–Mo oxide is formed which catalyzes hydrogen evolution generated by citrate evolution [9]. Podlaha *et al.* developed a mathematical model in which they considered that the discharge occured via a Ni–Mo intermediated species formed electrochemically or chemically and was catalysed by nickel [12, 14]. They did not take into account the interactions of the discharging components with hydrogen, but only considered hydrogen evolution from the decomposition of water. In agreement with

Degrez's results for the electrodeposition of Ni–Mo alloys from pyrophosphate solutions [10], we showed that the discharge of molybdenum inhibits nickel deposition, the inhibition being mass controlled (Figs 2 and 4). In addition the non-monotonic partial polarization curve for hydrogen evolution (Figs 1 and 6) shows that hydrogen participates in the discharge process and not only comes from water decomposition. The impedance investigation shows that the charge transfer processes occur through a porous layer, as in the Ni–Mo system.

References

[1] W. Z. Friend, *in* 'Corrosion of Nickel and Nickel Alloys', Wiley–Interscience, New York (1980), p.95–135 and p.248.
[2] E. Beltowska-Lehman, E. Chassaing and K. Vu Quang, *J. Appl. Electrochem.* **21** (1991) 606.
[3] E. Beltowska-Lehman, P. Ozga and E. Chassaing, *Surf. Coat. Technol.* **78** (1996) 233.
[4] A. Brenner, 'Electrodeposition of Alloys', vol. 1, Academic Press, New York/London (1963) p. 40.
[5] D. Landolt, *Electrochim. Acta* **39** (1994) 1075.
[6] F. A. Kroeger, *J. Electrochem. Soc.* **125** (1978) 2028.
[7] H. Fukushima, T. Akiyama, S. Akagi and K. Higashi, *Trans. Jpn. Inst. Met.* **20** (1979) 359.
[8] E. Chassaing, K. Vu Quang and R. Wiart, *J. Appl. Electrochem.* **17** (1987) 1267.
[9] *Idem, ibid.* **19** (1989) 839.
[10] M. Degrez and R. Winand, *Oberfläche-Surface* **8** (1990) 8.
[11] J. Crousier, M. Eyraud, J. -P Crousier and J. -M. Roman, *J. Appl. Electrochem.* **22** (1992) 749.
[12] E. J. Podlaha and D. Landolt, *Proc. Electrochemical Soc.* **94-31** (1994) 71.
[13] *Idem*, *J. Electrochem. Soc.* **143** (1996) 885.
[14] *Idem*, *ibid.* **143** (1996) 893.
[15] P. G. Daniele, G. Ostacoli, C. Rigano and S. Sammartano, *Trans. Met. Chem.* **9** (1984) 385.
[16] R. Y. Ying, *J. Electrochem. Soc*. **135** (1988) 2957.
[17] A. Surila and B. Szironene, *Soviet Electrochem.* **28** (1992) 1756.
[18] T. I. Quickenden and X. Jiang, *Electrochim. Acta* **29** (1984) 693.
[19] A. Samotus, A. Kanas, M. Dudek and R. Grybos, *Trans. Met. Chem.* **16** (1991) 495.
[20] H. Kaiser, K. D. Beccu and M. A. Gutjahr, *Electrochim. Acta* **21** (1976) 539.